Experimental Investigation and High Resolution Simulator of In-Situ Combustion Processes

Quarterly Report

Start date: April 2005
End date: June 2005

Margot Gerritsen
Anthony R. Kovscek

July 2005

DE-FC26-03 NT15405

Department of Petroleum Engineering
Stanford University
Green Earth Sciences Building
367 Panama Street
Stanford, CA 94305-2220

Abstract

Accurate simulation of in-situ combustion processes is computationally very challenging because the spatial and temporal scales over which the combustion process takes place are very small. In the last report, we focused heavily on experimental work. The experimental work is being continued and new combustion tube runs will be discussed in the next quarterly report. In this current and **seventh** report, we will focus on our research in numerical methods. In the previous reports, we discussed in detail the development of our adaptive parallel pressure solver, which is based on an efficient Cartesian Adaptive Mesh Refinement technique. This methodology allows much higher grid densities to be used near typical fronts than current simulators. Last quarter we improved the computation of upscaled permeabilities. This quarter we derived a method to compute accurate transmissibilities. We present preliminary results in this quarterly report. We have also started the development of a Virtual Kinetic Cell (VKC) that we will use to test numerical methods for solving the kinetics in combination with phase behavior. A discussion of the approach followed is included.
.

July 2005

Table of Contents

List of graphical materials

1. Introduction

In-situ combustion, or air injection, is the process of injecting oxygen into oil reservoirs to oxidize the heaviest components of the crude oil and enhance oil recovery through the heat and pressure produced. The emphasis of this work is to study and model numerically in situ combustion processes. The ultimate objectives are to provide a working accurate, parallel in situ combustion numerical simulator and to better understand the in-situ combustion process when using metallic additives and/or solvents combined with in situ combustion. For this purpose, experimental, analytical and numerical studies are conducted.

This report presents results of the third quarter of the second year of this project. In this report we focus on the computational program.

2. Executive Summary

2.1. Personnel

Current personnel include Prof. Margot Gerritsen (PI), Prof. Tony Kovscek (Co-PI), Dr. Louis Castanier (Technical manager), Dr. Jonas Nilsson (postdoctoral fellow), Mr. Rami Younis (PhD student), and Mr. Qing Chen (MSc student). Mr. Jean Cristofari (MSc student) is also working on the project, albeit paid from departmental sources. We have also had the pleasure this quarter of having Mr. Morten Kristensen with us from the Technical University of Denmark as visiting scholar supported from departmental sources. He is staying with us for a period of six months.

2.2. Important accomplishments

2.2.1 Adaptive parallel pressure solve with appropriate multi-level upscaling

In-situ combustion processes involve several coupled physical processes with a wide range of characteristic spatial and temporal scales. For reliable performance prediction it is essential to accurately represent reservoir heterogeneity, as the highly mobile phases will seek the high permeability flow paths, greatly affecting global sweep. We propose to use aggressive grid adaptivity to accurately model important physical processes with small spatial support, such as the kinetics in the very thin combustion zones.

As discussed in previous quarterly reports, we developed a cell-based Cartesian refinement strategy, which we refer to as the Cartesian Cell-based Anisotropic Cell Refinement (CCAR) method. For increased computational efficiency we allow anisotropic refinements. The strategy is explained in detail by J. Nilsson, *et al* [1].

Effective upscaling for CCAR grids

For coarse Cartesian methods static or local upscaling methods are not optimal for EOR processes. For such processes, it is important to resolve high permeability connected flow paths well since the highly mobile gases will seek these paths. If some sort of global connectivity is not introduced (which is not the case in static or local upscaling methods) one can never expect these to be well represented.

In static upscaling, the permeability in a coarse cell is computed from algebraic averages of underlying finescale permeability values. When a coarse grid cell is not aligned with, but rather straddles a strong permeability contrast, this averaging can results in a strong smoothing of the permeability field. The same holds true for local or extended local methods [2]. For flow-based grids on the other hand, these local upscaling methods may lead to good results provided the grids capture the reservoir heterogeneity well.

It has been shown that for Cartesian methods, the local-global method leads to improved results as compared to local, or extended local, methods. For each coarse grid cell, an effective permeability is computed by solving a local flow problem on the fine geo-cellular grid directly around the coarse cell. This local flow problem is driven by boundary conditions interpolated from a coarse global solve. The resulting coupling between the local flow problems and the coarse global solve leads to an iterative scheme that generally converges rapidly.

Local-global upscaling

For the coarse global solves, we solve one flow problem corresponding to each coordinate direction, with generic boundary conditions: a constant pressure difference in the given coordinate direction, and no flow across boundaries corresponding to the other directions. In the following description of the algorithm for a 2D domain $[0,l_x]$ x $[0, l_y]$, we denote by p_x a pressure field that is constant for x=0 and x= l_x, with no flow across y=0 and y= l_y. The pressure field p_y satisfies analogous boundary conditions.

```
while not converged do
    for each coarse cell C_i do
        if first iteration then
                Use generic boundary conditions: constant pressure in one coordinate direction,
                no-flow in all other coordinate directions
        else
                Use interpolation of global solutions to approximate pressure on ∂E_i
                Use Dirichlet boundary conditions using these pressure values
        end
        Solve pressure equation on E_i with Dirichlet data obtained from interpolated values
        Define a Cartesian grid G_i on E_i containing C_i as a cell
        Compute fluxes between cells of G_i and pressure values at cell centers of G_i
        Use fluxes and pressure values on G_i to compute new permeability tensor K_i for C_i
    end
    Solve generic flow problems on G to obtain pressure fields p_x and p_y
    Check for convergence
done
```

Upscaling to the Base CCAR Grid

The base CCAR grid is designed with the aim of preserving high permeability flow paths, in view of their importance in EOR applications. By accounting for these paths, we hope to minimize upscaling errors that can occur when such features are lost due to coarsening. The local-global method fits very naturally in this coupled process, since its consistency check between the coarse and fine grids can be used to ensure that the effects of fine-scale features are properly accounted for in the coarse-scale model.

We apply as a first static refinement indicator, the method proposed by Younis and Caers [3]. The method is based on a 'leaky' connected-set approach that delineates clusters of fine cells with similar permeability. Heuristic measures are used to color each connected set, indicating the level of the importance of capturing the set by refinement. Refinement flags are then obtained by explicit boundary detection. An illustration of the process appears in Figure 1. In the current implementation, a minimum level of refinement is set based on the resolution of the geocellular grid and efficiency considerations, and a CCAR grid G is generated by iteration until these level constraints are met. Such a grid is illustrated in Figure 2.

After these initial steps, we apply local-global upscaling to each level of refinement in sequence, starting at one level above the geo-cellular level (there is no need to consider the geo-cellular level, since it already has permeability values). When appropriate permeability values have been found on a level, we fix them and continue on to the next coarser level. This multi-level local-global procedure is repeated until the permeability field on the CCAR grid G has converged. It should be noted that it is not necessary to begin by upscaling to a refinement level that is almost

as fine as the geocellular grid. Instead, we can upscale to a coarser Cartesian grid, and then upscale to individual cells in the CCAR grid that are of a finer scale.

While it is possible to upscale to all cells of the CCAR grid at once, instead of processing them one level at a time, this is not advisable. Allowing permeability tensors in neighboring cells of different levels to vary from iteration to iteration may lead to unwanted smoothing of permeability across such cells. This may cause permeability contrasts to be lost, degrading the accuracy of global flow.

As the CCAR grid is adapted, either as a result of excessive upscaling error or dynamic adaptation during transport, the hierarchy of permeability fields is examined to determine if permeability values have already been computed for cells that have been added to the grid. If so, then the new cells are simply populated with these values. Otherwise, we compute the needed values by upscaling to the new cells, as in the previously described algorithm for upscaling to the base grid. Permeability values in all other cells are fixed, and values in the new cells are computed in such a way as to preserve flow through the cells at the next finer scale that they contain.

Transmissibility Upscaling

A multi-level approach can also be used to upscale transmissibility to a CCAR grid. The algorithm proceeds as in permeability upscaling, except that extended regions are face-centered instead of cell-centered. At each level, faces of successively larger area are processed.

In Figure 3, we illustrate how we approximate the transmissibility across the left face of the cell centered at the point c_1. We choose an extended region centered at this face large enough to contain the cells centered at the points c_1, c_2 and c_3. For i=1, 2, 3, let these cells have dimensions h_x^i and h_y^i, and diagonal permeability tensors with diagonal elements k_x^i and k_y^i. The area of the face of cell i that borders the face of interest is denoted by A_i

We solve the pressure equation on the extended region with Dirichlet boundary conditions as in permeability upscaling. Let p_1, p_2 and p_3 be the averages of the pressure on the corresponding cells. Then the flux across the face is given by

$$flux = -2\,h_y^1 \frac{h_y^1\,p_1 - h_y^2\,p_2 - h_y^3\,p_3}{\frac{h_x^1 h_y^1}{k_x^1} + \frac{h_x^2 h_y^2}{k_x^2} + \frac{h_x^3 h_y^3}{k_x^3}} = -2A_1 \frac{A_1 p_1 - \sum_{i=2}^{3} A_i p_i}{W}$$

In this case, the permeabilities are unknown, but by computing the flux from the local solution, we can solve for $W = V_c/K_c + \sum V_i/K_i$. This value is then incorporated directly into the stencil of the pressure solver for the CCAR grid. Results on transmissibility upscaling are forthcoming.

2.2.2 The development of the Virtual Kinetic Cell (VKC)

Motivation

The spatial as well as temporal scales in in-situ combustion vary over many orders of magnitude. The bulk of the chemical reactions take place in a narrow reaction zone that may be less than a meter in thickness compared to reservoir scales of hundreds or thousands of meters. Moreover,

combustion reactions often occur in fractions of a second, whereas the temporal scales associated with convective transport may be running to days or years. In our simulator design, we aim to accurately predict field performance using a hierarchical approach, in which both spatial and temporal resolution are adapted.

A number of different processes may be identified in in-situ combustion, each having its own characteristic time scale. The standard formulation of the in-situ combustion equations include convective mass transfer, convective and conductive heat transfer, kinetically controlled chemical reactions and fluid phases in thermodynamic equilibrium [4,5,6]. The assumption of immediate phase equilibrium implies that the timescale for mass transfer between phases is faster than all other timescales. Of the remaining processes, the chemical reactions are likely to occur on timescales that are again much faster than the scales for mass and heat transport.

In order to capture the essential process dynamics in a numerical simulation, the reaction kinetics must be integrated using time steps that are much smaller than those necessary for capturing the effects of convection and conduction. One way to approach this problem numerically is to split the equations to separate convective and conductive terms from reaction terms. This was previously discussed in our quarterly reports. Each global time step then consists of a series of substeps, in which the individual terms are integrated in time separately. The immediate advantage of this approach is that time step sizes can vary between processes and are not dictated by the fastest scale present. In a reaction substep each grid block is effectively treated as a small chemical reactor or kinetic cell with homogeneous pressure and temperature and well mixed fluids.

We are building a Virtual Kinetic Cell (VKC) to study the interaction of chemical kinetics, phase behavior and numerical solution techniques. Our goals are to better understand the sensitivity of the kinetics to phase behavior and other process parameters (temperature, pressure, interaction with reservoir through diffusion, conduction and advection), the sensitivity to errors introduced by numerical methods, and ultimately develop accurate and efficient solution algorithms for the reaction/phase equilibrium substep to be used in an in-situ combustion simulator.

Conservation Equations

For our initial discussion we assume

- Three fluid phases (oil, gas, water), and one solid phase (coke).
- Thermal equilibrium between fluid phases, solid phases and rock. Fluid phases in thermodynamic equilibrium.
- Oil and water are immiscible.
- Only hydrocarbon components in the oil phase react with oxygen.

The total volume of the kinetic cell may be composed of solid rock matrix (r), oil phase (o), gas phase (g), water phase (w) and solid coke phase (c). The void porosity is defined as the fraction of the total volume occupied by fluids or solid coke

$$\phi_v = \left((V_f + V_c)/V\right).$$

Similarly, the fluid porosity is defined as the fraction occupied only by fluids. It may be expressed in terms of void porosity and solid coke concentration, c_c, as

$$\phi_f = \phi_v\left(1 - c_c/\rho_c\right),$$

in which ρ_c is the coke density.

The conservation of each chemical component is written as:

$$\frac{dn_i}{dt} = V\sum_{k=1}^{n_r} A_{ik} r_k + F_i^{in} - F_i^{out}, \quad i = 1,\ldots,n_c \ ,$$

in which r_k is the reaction rate for reaction k, A_{ik} the stoichiometric coefficient of component i in reaction k (negative for reactants and positive for products) and F^{in} and F^{out} the molar flowrates of component i in and out of the cell, respectively. The energy conservation equation is:

$$\frac{dU}{dt} = V\sum_{k=1}^{n_r} -\Delta H_k r_k + H^{in} - H^{out} + Q^{ext},$$

in which ΔH_k is the reaction enthalpy for reaction k and H^{in} and H^{out} are the fluxes of enthalpy in and out of the cell. Q^{ext} represents a heat source/sink term due to external heating or cooling. Finally, U is the total internal energy of the system expressed as

$$U = V(1-\phi_v)U_r + n_o U_o + n_g U_g + n_w U_w + n_c U_c.$$

Here, U_r is the volumetric internal energy of rock and U_j is the molar internal energy of phase j, $j \in \{o,g,w,c\}$. All inflow terms in the above equations may depend on time, but are assumed known. The energy heat source/sink is modeled as:

$$Q^{ext} = UA(T_r - T),$$

in which T_r is the heating/cooling temperature and UA is an overall heat transfer coefficient. The cell may be operated in a `constant volume' or a `constant pressure' mode. For constant pressure there is no outflow from the cell, and the cell volume is allowed to expand to match the sum of the fluid, coke and rock volumes. For constant volume, on the other hand, gases are allowed to leak out of the cell when volume changes occur due to chemical reactions and temperature changes. When only components in the gas phase can leave the cell, the molar flow rates in may be expressed as

$$F_i^{out} = Q^{out}\rho_g y_i,$$

where ρ_g is the gas density and Q^{out} is the volumetric flow rate, which is taken proportional to the difference between the cell pressure and the external pressure

$$Q^{out} = k_v(p - p^{ext}).$$

Here, k_v denotes a valve coefficient. Since the pressure is treated as a variable in the constant volume formulation, an additional equation must be specified, which is given by a constraint on the phase volumes.

In this preliminary VKC model, we use simple K-value correlations to describe phase behavior. In later versions the VKC model will be extended to include more accurate phase behavior with composition dependent K-values obtained from an equation of state.

Rock and solid component densities are assumed constant. The water phase density is correlated with temperature and pressure. The oil phase density is obtained by ideal mixing of pure component densities. The gas phase density is calculated from the Redlich-Kwong equation of state using linear mixing rules and zero interaction coefficients.

Rock and solid component internal energies are computed using constant heat capacities. Fluid phase internal energies are computed from heat capacity and vaporization enthalpy correlations. Ideal mixing of component enthalpies is assumed (similar implementation as in the commercial STARS simulator [4]).

3. Experimental

Our experimental program is not reported on this quarter. It was extensively discussed in the previous report and will be included again in the next quarterly.

4. Results and discussion

This report covers the seventh quarter of our research grant. The quarter was used primarily to further design the computational algorithms, with increased emphasis on the three-dimensional simulator, and to continue our experimental work. We have made good progress in these areas again this quarter. In this report we focus almost exclusively on the numerical results. A paper on our work on the multi-level upscaling was accepted for presentation at the SPE Annual Technical Conference and is attached to this report. An abstract submitted to the Heavy Oil and Thermal Recovery conference in Calgary this coming October was also accepted. The paper will be presented by Rami Younis.

4.1. Adaptive pressure solve and multi-level upscaling

An implementation of the multi-level local-global upscaling algorithm has yielded encouraging results. When upscaling a channelized domain from a fine grid of 4096 cells to a CCAR grid containing 1345 cells, we obtain a good match with fine grid global flow for generic flow problems in both the x- and y-directions, whereas local-global upscaling only produced a good match in the *x*-direction, as indicated in the following table.

Algorithm and resolution	% Error in Q_x	% Error in Q_y
Local-global, uniform grid, 1024 cells	1.78	8.62
Multi-level local-global, CCAR, 1345 cells	2.29	1.02

In Figure 4, the fine permeability field is compared to the “effective” permeability field obtained by the ratio of the magnitude of the velocity and the pressure gradient on each fine cell, for a generic global flow problem solved on the coarse scale using the computed upscaled permeability.

Our upscaling approach, in combination with CCAR, leads to reduced process dependency. Using a base CCAR grid containing 445 cells, we solve the pressure equation with flow originating from a corner of the domain. We then compare the global flow to that obtained by solving the same problem using a Cartesian grid containing 512 cells using local-global upscaling. The results are listed in the following table. Note that local-global upscaling on the Cartesian grid only yields high accuracy in one case, while the accuracy multi-level local-global upscaling on the CCAR grid yields is much less dependent on the boundary conditions.

Corner	% error, 512-cell, local-global	%error, 445-cell MLLG
Lower left	14.68	6.95
Upper left	1.19	2.55
Lower right	11.01	4.71
Upper right	12.49	6.27

The upscaled permeability fields are illustrated in Figure 5. As can be seen in the figure, the channels are more accurately resolved by upscaling on the CCAR grid.

4.2. Virtual Kinetic Cell

The kinetic cell model handles any number of hydrocarbon components and inert gas components along with the water component. A specific example is considered here consisting of a total of 6 components and four reactions. The components are light oil (LO), heavy oil (HO), oxygen (O_2), inert gas (IG), coke C and water (H_2O). Three types of reactions are considered: (1) oxidation of hydrocarbon components in the oil phase, (2) cracking of hydrocarbon components forming solid coke, and (3) oxidation of coke.

$$\begin{aligned} LO + O_2 &\rightarrow IG + H_2O \\ HO + O_2 &\rightarrow IG + H_2O \\ HO &\rightarrow LO + C + IG \\ C + O_2 &\rightarrow IG + H_2O \end{aligned}$$

The reaction rates are expressed as

$$\begin{aligned} r &= k(T)p\,y_{O_2}(\phi_f s_o \rho_o x_i), && \text{HC oxidation} \\ r &= k(T)(\phi_f s_o \rho_o x_i), && \text{HC cracking} \\ r &= k(T)p\,y_{O_2}(\phi_v c_c), && \text{coke oxidation} \end{aligned}$$

in which y_{O2} is the gas molefraction of oxygen and x_i is the oil phase molefraction of component i, $i \in \{LO,HO\}$. The reaction constants are modeled using an Arrhenius expression

$$k_k(T) = \alpha_k e^{-E_k/RT},$$

in which α_k and E_k are the frequency factor and activation energy for reaction k, respectively.

A simulation is carried out with an initial amount of air and heavy oil in the reactor. Air is also fed continuously to the reactor at a rate of 0.01m³/hr and a temperature of 473K. Initial conditions are specified in Figure 6 along with the simulation results. Other key parameters are given in the table below.

Reaction Parameters			
Reaction	**α (1/(hr.atm)) ***	**E (kJ/mole)**	**(-ΔH) (kJ/mole)**
LO oxidation	$4.44\ 10^{11}$	$1.38\ 10^{5}$	6763
HO oxidation	$4.44\ 10^{11}$	$1.38\ 10^{5}$	29132
HO cracking	$4.17\ 10^{5}$	$6.28\ 10^{4}$	93
Coke oxidation	$6.13\ 10^{3}$	$5.86\ 10^{4}$	523
Other Parameters			
p^{ext}	137 atm	ϕ_v	0.4
UA	25 kJ/(hr K)	Q_{inj}	0.01 m^3/hr
T_r	473 K	T_{inj}	473 K
k_v	0.001 m^3/(hr atm)		

Three different reaction regimes are observed from Figure 6. Initially heavy oil cracking dominates leading to a build-up of light oil and coke. The relatively small heat of reaction associated with heavy oil cracking causes only a small temperature increase at this stage. At t=6hrs the light and heavy oil oxidation reactions kick in causing a large temperature increase. The final stage of the process is mainly coke oxidation and the temperature decreases and levels around the cooling temperature. The small bumps observed in the water and oxygen curves are associated with formation of a hydrocarbon gas phase.

5. Conclusions

5.1. Adaptive flow solver with multi-level local-global upscaling

We have developed an upscaling method that not only ensures consistency between the coarse and fine scale models, but also uses aggressive adaptation to produce a coarse scale model that contains far fewer grid points than would be required when using a Cartesian grid to achieve the same accuracy during simulation.

Our approach of tightly integrating adaptivity with upscaling is particularly suited to compositional and non-isothermal recovery methods, which involve several coupled physical processes with a wide range of characteristic spatial and temporal scales. It is of utmost importance to resolve the potential connected high-permeability flow paths in order to accurately determine the sweep efficiency and breakthrough times of these processes.

The results are very encouraging, as indicated in the tables included in the previous sections. These results suggest that refinement is an effective means to control upscaling errors and reduce process dependency.

On Cartesian grids, transmissibility upscaling typically yields more accurate coarse scale models than permeability upscaling, as demonstrated in the case of local-global upscaling. Using face-

centered extended regions, multi-level local-global upscaling can be applied to compute transmissibilities on CCAR grids.

The integrated approach we propose in this paper closely couples upscaling and adaptivity. If the grid is adapted, the coarse-scale permeability field can easily be updated to maintain consistency with global flow, and this updating process can be accomplished with minimal effort, involving only local computations in most cases. This ease of updating naturally suggests an iterative process in which the grid is adapted based on estimates of local upscaling error.

Our approach of upscaling to cells of one refinement level at a time, while most natural for CCAR grids, can just as easily be applied to other types of grids. Future work will include generalization of our algorithm to other gridding strategies such as patched refinements, unstructured grids, or curvilinear grids. In addition, the algorithm will be implemented on 3D domains, as well as multiphase flow problems.

5.2. Virtual Kinetic Cell

We started the development of a Virtual Kinetic Cell, a software code that allows simulation of kinetics taking place in a kinetics cell experiment. Boundary conditions are general and can be used to mimic interaction with the reservoir.
The main goal of this work is to allow comparison of numerical methods, and investigate the interplay between numerics and simulated physics. In particular we are interested in designing appropriate numerical approaches for the multi-scale processes in a kinetics cell and the interaction between kinetics and phase behavior.
Computational efficiency is not our priority at the moment. Once the VKC is working properly and a good numerical approach has been found, we will focus on computational efficiency before implementing the methods in our in-situ combustion simulator.
The VKC package will be made available to the public once completed. We expect this development to take another 3 or 4 months.

References

1. J. Nilsson, M. Gerritsen, R. Younis, “A Novel Adaptive Anisotropic Grid Framework for Efficient Reservoir Simulation,” *Proc. of the SPE Reservoir Simulation Symposium*, 2005, SPE 93243
2. Y. Chen, L. Durlofsky, M. Gerritsen and X.H. Wen, "A coupled local-global upscaling approach for simulating flow in highly heterogeneous formations", Advances in Water Resources, 26:1041-1060, 2003
3. R.M. Younis and J. Caers, "A Method for Static-based Upgridding," *Proc. of the 8th European Conference on the Mathematics of Oil Recovery*, Sept. 2002
4. *STARS Advanced Process and Thermal Reservoir Simulator*, Computer Modeling Group Ltd, 2004
5. K. H. Coats, “In-Situ Combustion Model”, *Society of Petroleum Engineers Journal*, 269, 533-554, 1980
6. R.B. Crookston, W.E. Culham, and W.H. Chen, “A Numerical Simulation Model for Thermal Recovery Processes”, Society of Petroleum Engineers Journal, 37-58, 1979

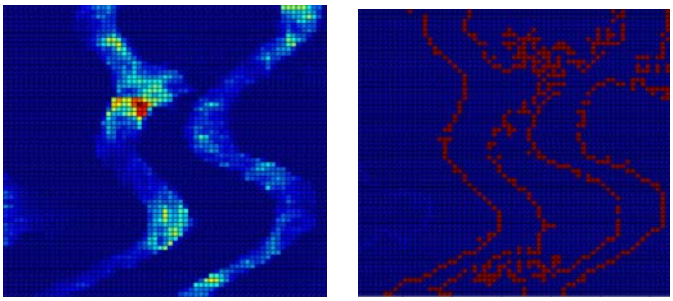

Figure 1: Permeability field (left), and boundaries of connected flow paths detected by leaky connected-set approach (right)

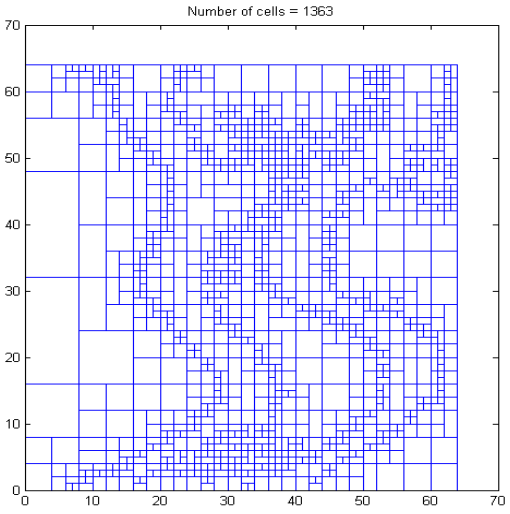

Figure 2: base CCAR grid generated from permeability field and connected sets from Figure 1

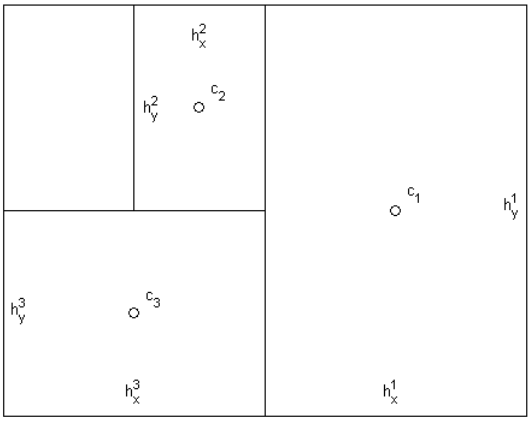

Figure 3: the properties of the cells centered at c_1, c_2 and c_3, along with the pressure values at these points, are used to compute the flux across the left face of the cell centered at c_1.

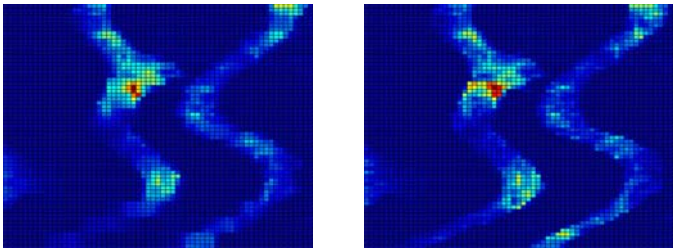

Figure 4: Left, fine permeability field for channelized reservoir. Right, "effective" permeability, defined by $||v||/||\nabla p||$ on each fine cell, where v and p are obtained from pressure solve using upscaled permeability field.

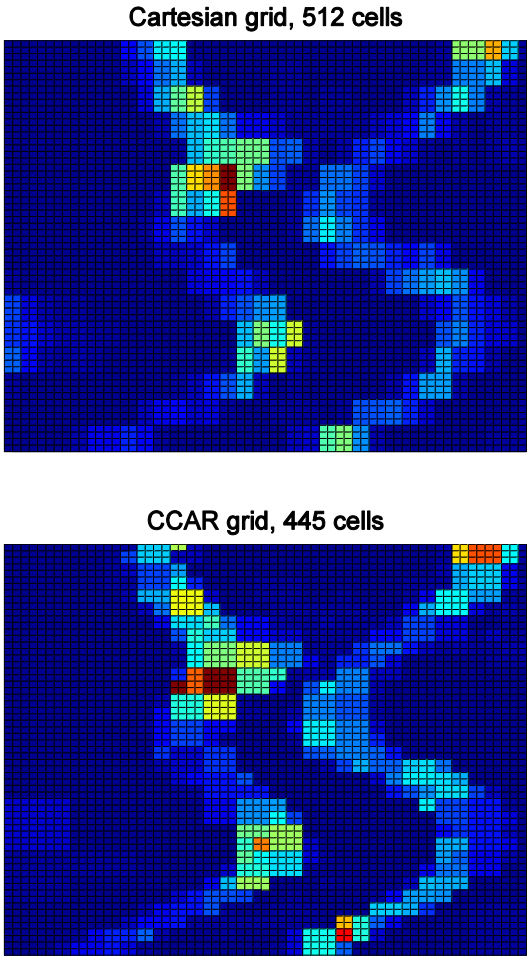

Figure 5: Top, upscaled permeability field generated by local-global upscaling on a 512-cell Cartesian grid. Bottom, upscaled permeability field generated by multi-level local-global upscaling on a 445-cell CCAR grid.

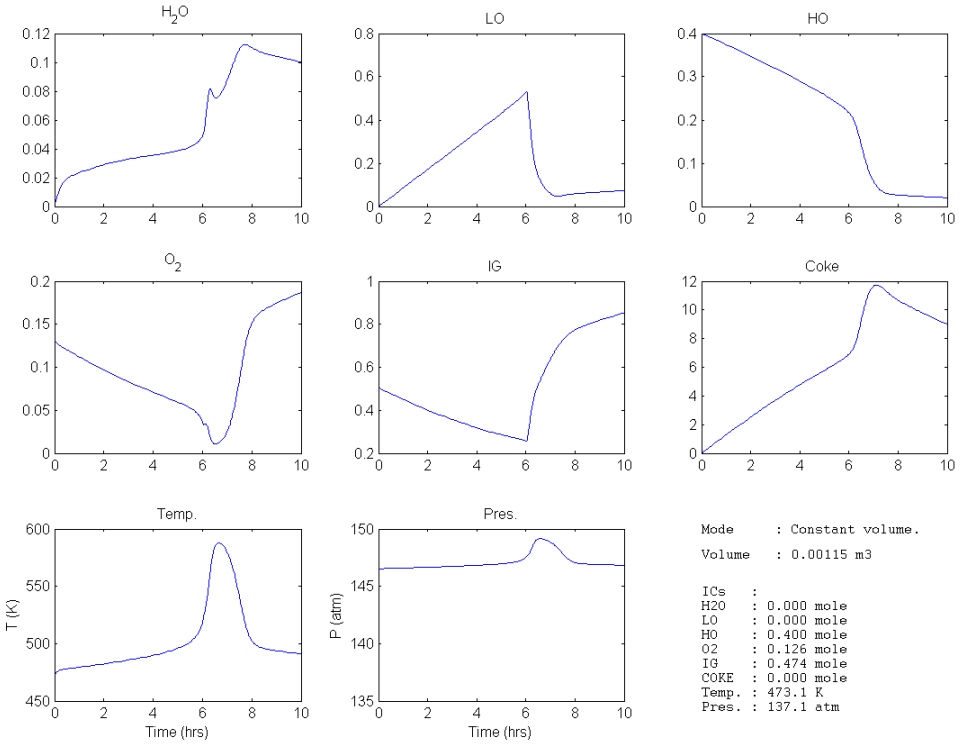

Figure 6: Results from the VKC simulation example. The initial conditions are listed.